A New Formula Assignment Algorithm for the Deuterium Labeled Ultrahigh-Resolution Mass Spectrometry: Implications to the Formation Mechanism of Halogenated Disinfection Byproducts

Qing-Long Fu[1, 2], Manabu Fujii[2*], Akari Watanabe[2], Eunsang Kwon[3]

[1] School of Environmental Studies, China University of Geoscience, Wuhan 430074, China.

[2] Department of Civil and Environmental Engineering, Tokyo Institute of Technology, 2-12-1, Ookayama, Meguro-Ku, Tokyo 152-8550, Japan.

[3] Research and Analytical Center for Giant Molecules, Graduate School of Science, Tohoku University, 6-3 Aoba, Aramaki, Aoba-Ku, Sendai 980-8578, Japan.

**E-mail: fujii.m.ah@m.titech.ac.jp*.

ABSTRACT

The ultrahigh-resolution mass spectrometry (UHR-MS) coupled with isotope labeling is of increasing attentions in elucidating the transform mechanisms of dissolved organic matter (DOM). However, there is a paucity of automated formula assignment algorithm applicable to halogenated disinfection byproducts (X_n-DBPs), particurally for iodinated organic compounds, and deuterated DOM . Herein, for the first time, we have developed a novel formula assignment algorithm based on deuterium-labeled UHR-MS, namely FTMSDeu, and the algorithm was applied to determine precursor molecules of X_n-DBPs and evaluate the relative contribution of electrophilic addition and electrophilic substitution reactions in X_n-DBPs formation according to the hydrogen/deuterium exchange of DOM molecules. Furthermore, tandem mass spectrometry with homologous-based network analysis was employed to validate the formula assignment accuracy (41%) of FTMSDeu for iodinated disinfection byproducts (I_n-DBPs). And the remaining I_n-DBPs compounds were assigned with the empirical rule of minimum number of non-oxygen heteratoms. The electrophilic substitution accounted for 82%-98%, 71%-89%, and 43%-45% of X_n-DBPs formation for X_n-DBPs containing chlorine, bromine, and iodine, respectively, manifesting the dominant role of electrophilic substitution in chlorine disinfection under conditions of low bromine and iodine concentrations. The absence of presumed X_n-DBPs precursors in some treatments in this study also suggests that X_n-DBPs formation include secondary reactions (*e.g.*, oxidation, hydrolysis) in addition to electrophilic addition and/or substitution of halogens. These findings highlight the significance of isotopically labeled UHR-MS techniques in revealing the transformation of DOM in natural and engineered systems.

INTRODUCTION

Natural organic matter (NOM) is a ubiquitous mixture of complex organic compounds from the abiotic and biotic degradation of living organic matter [1], playing important roles as precursors for halogenated disinfection byproducts (X_n-DBPs, where X represents halogen atoms including chlorine [Cl], bromine [Br], and iodine [I], and *n* is the number of halogen atoms) in terrestrial and aquatic environments [2,3]. Due to the extremely diverse nature of NOM, it was challenging to elucidate their chemical composition at the molecular level until the employment of ultrahigh-resolution mass spectrometry (UHR-MS), particularly the Fourier-transform ion cyclotron resonance mass spectrometry (FTICR-MS) [4,5]. Since its first application to NOM study [6], FTICR-MS has been widely adopted to characterize the complexity of NOM in the last two decades through the development of automated molecular formula assignment methods such as the in-house code from Kujawinski and Behn[7], MassCal [8], Formularity software[9], MFAssignR[10], ICBM-OCEAN[11], and the TRFu code[12]. Moreover, FTICR-MS with stable isotope labeling has initiated the new possibilities of quantifying the number of labile H and O and structural information such as ether O atoms, carboxyl and hydroxyl functional groups in individual molecules of NOM [1,13-15], further refining compound aromaticity [16], and relation of NOM molecular structures with optical property[17]. However, data interpretation of stable isotope-labeled UHR-MS spectra remains challenging, and only a few methods have been developed to address the formula assignment for stable isotope-labeled UHR-MS spectra. For example, the Transhums software is capable of solving the formulae to NOM molecules labeled with deuterium (D) and ^{18}O, respectively [1,14], but it only considers C, H, and O atoms in the formulae calculation.

The H atoms involved in the acid-base reactive moieties of NOM molecules (*e.g.*, carboxyl and hydroxyl groups) can be readily exchanged by D in solution at diffusion-limited rate (referred

as to "labile H") [13,18]. In contrast, when H atoms are incorporated into the structural backbone (referred as to "backbone H"), the H/D exchange generally require activation of the molecules such as acid-, base-, or metal-mediated catalysis and chemical ionization at high temperature [19]. Given the pronounced acidic nature of acid-base functional groups in NOM molecules [20,21] and the fact that the H/D exchange rate for the labile H is much faster than for the backbone H [19], it would be reasonable to assume that the carboxyl and hydroxyl groupd containing labile H account for the majority of the H/D exchange sites for NOM in the D_2O system. The resultant labile D in deuterated NOM molecules could be reversibly exchanged with H in the H_2O system.

X_n-DBPs are inevitably formed by the interaction between halogens and NOM during chlorination (*e.g.*, NaClO treatment) and of great concern in water and wastewater treatment due to their toxic effects on human and aquatic organisms [22-24]. Chlorination of natural and engineered waters containing bromide and iodide may unintentionally yield brominated and iodinated byproducts (Br_n-DBPs and I_n-DBPs, respectively), which are more toxic than chlorinated byproducts (Cl_n-DBPs) [24]. The Cl and Br atoms in hypochlorite (OCl^-) and hypobromite (OBr^-) have strong electrophilic properties, and readily react with the abundantly present unsaturated functional groups in NOM molecules mainly via electrophilic substitution and electrophilic addition, followed by secondary reactions such as oxidation, hydrolysis and decarboxylation [25-28]. While electrophilic substitution is considered to be major pathway in the formation of X_n-DBPs (compared to electrophilic addition) during disinfection process due to its higher reaction rate [26,28], it is still challenging to quantify their relative contributions primarily because of the high complexity of NOM and associated reactions as well as lack of techniques to identify such system at molecular level. For example, there is a difference in chemical formula of products between electrophilic substitution ($-n$H$+n$X) and addition ($+n$OH$+n$X) for the identical precursor. Thus the

absolute atom difffernece between their corresponding precursors of a given X_n-DBPs was integer number of H_2O, which was a typical formula building block for NOM molecules (Figure S1)[29-31].Furthermore, when disinfection is performed in the D_2O system with NOM, the electrophilic substitution and addition could be distinguished according to the number of D involved in products, as shown in Eqs. 1-3.

$$OX^- + D_2O \leftrightarrow DOX + OD^- \quad (1)$$

$$C_xH_yO_z + n\mathrm{DOX} \xrightarrow[substitution]{Electrophilic} C_xH_{y-n}O_zX_n + n\mathrm{HOD} \quad (2)$$

$$C_xH_yO_z + n\mathrm{DOX} \xrightarrow[addition]{Electrophilic} C_xH_yD_nO_{z+n}X_n \quad (3)$$

where XO^- and $C_xH_yO_z$ represent hypohalite ions and NOM molecules, respectively. In case of the labile D in X_n-DBPs formed via electrophilic substitutation, D will be readily replaced by H when solutions were subjected to H_2O (particurally such reaction can be facilitated under acidic condition [*e.g.*, pH ~2]). In contrast, electrophilically added D in X_n-DBPs (*i.e.*, Eq 3) will remain intact under the identical condition [14].

Recently, UHR-MS techniques have enabled high-throughput non-target screening of X_n-DBPs species, including hundreds to approximate three thousand DBPs species [32-39]. In our previous study, accuracy of formula assignment for Cl_n-DBPs and Br_n-DBPs was improved up to 97% by accounting for distinct isotopic patterns of Cl and Br in addition to three optional rules [40]. However, an automatic formula assignment algorithm for I_n-DBP is not yet available, partly because there is only one naturally occurring stable isotope of iodine (*i.e.*,^{127}I). Furthermore, UHR-MS coupled with D isotope labeling approach is expected to be a valuable tool to improve the accuracy of molecular assignment of X_n-DBPs including I_n-DBPs. This technique could also be

useful to quantify the contribution of electrophilic substitution and addition in the formation of X_n-DBPs and to trace their direct precursors. However, an effective formula assignment method is still required to automatically analyze non-oxygen heteroatoms-containing molecules (*e.g.*, X_n-DBPs) for the isotope-labeled UHR-MS spectra of dissolved organic matter (DOM) in natural and engineered environments.

The main objectives of this study were (i) to develop a new formula algorithm to assign formulae to NOM and X_n-DBPs labeled with D (where X is Cl, Br or I), and (ii) to apply the developed algorithm to quantify the contribution of reaction mechanisms (*i.e.*, electrophilic substitution and addition) for X_n-DBPs at individual molecular level. The relevant results will provide valuable insights into algorithm development for UHR-MS spectra labeled with other isotopes such as ^{13}C and ^{18}O and elucidate further details in the formation mechanisms of X_n-DBPs.

METHODS AND MATERIALS

Sample preparation. The Suwannee River NOM (SRNOM [2R101N] purchased from International Humic Substances Society) was prepared at concentration of 50 mg-C/L in 10 mL D_2O (99.8%, Kanto Chemical, Japan). The SRNOM solution was then chlorinated with 50 mg/L NaClO (Kanto Chemical, Japan) in the absence and presence of 5.0 mM potassium bromide (>99.0%, Sigma-Aldrich, USA) or 1.0 mM potassium iodide (>99.0%, Sigma-Aldrich, USA). Thus, following three samples were prepared: i.e., (i) ClO^- + NOM in D_2O (referred to as "Treatment A"), (ii) ClO^- + Br^- + NOM in D_2O ("Treatment B"), and (iii) ClO^- + I^- + NOM in D_2O ("Treatment C"). All samples were then incubated for a week at room temperature under the dark condition. The chlorination reactions were terminated by adding excess Na_2SO_3 (>99.0%, Kanto

129 Chemical, Japan). Due to the limited availability of D_2O, concentrations of aforementioned
130 chemicals were set at approximately ten times the dose of ClO^- typically used in water treatments
131 and ten times the environmentally relevant concentrations of dissolved organic carbon, Br^- and I^-
132 [27,41-43]. The pH values for Treatments A, B, and C were determined to be 8.11, 8.93, and 7.81 at
133 the bigining of the treatment, and 6.20, 6.30, and 5.08 at the end of the treatment (*i.e.*, after one
134 week), respectively.

135 After the treatment, the samples were diluted to 250 mL with ultrapure water (Milli-Q, ≥15
136 MΩ·cm), followed by the solid-phase extraction (SPE) for dissolved organic matter (DOM) using
137 the method reported elsewhere [44]. Briefly, all diluted samples were acidified with concentrated
138 HCl (Ultrapure Regent, Kanto Chemical, Japan) at pH ~2 and then gravitationally passed through
139 Bond Elut PPL cartridges (1g and 6 mL, Agilent) which were activated and rinsed with 12 mL
140 methanol (MeOH, LC-MS grade, Kanto Chemical, Japan) and 6 mL Milli-Q water, respectively.
141 The cartridge was then rinsed with 20 mL HCl (pH ~2.0) and 6 mL Milli-Q water to desalt and
142 remove residual Cl^-, respectively, followed by complete drying using N_2 gas (99.9% gas purity).
143 DOM was finally eluted with 6 mL MeOH and diluted twofold with Milli-Q water. Separately,
144 two SRNOM standard solutions (200 mg-C/L) were prepared by dissolving SRNOM in Milli-Q
145 H_2O and deuterium oxide (D_2O), respecitivey (referred to as H-SRNOM and D-SRNOM) and used
146 to examine exchange of labile H/D in NOM molecules. The H-SRNOM and D-SRNOM solutions
147 were further diluted twofold with MeOH and MeOD (99.5% D, Sigma-Aldrich, USA),
148 respectively.

149 Additional chlorination treatment (Treatment D) was performed to examine the applicability
150 of newly developed algorithm (namely FTMSDeu) to the formula assignment of I_n-DBPs by using
151 FTICR-MS/MS and network analysis. To this end, the sample was prepared at concentrations of

2.5 mg-C/L for SRNOM, 50 mg/L for ClO^- and 200 mg/L for I^-, and incubated for a week at room temperature under the dark. In this sample, high I^- concentration was employed to generate high-intensity for I_n-DBPs in the FTICR-MS/MS analysis. The samples were subjected to SPE-based DOM extraction by using aforementioned procedure.

All samples were stored in the dark at 4˚C and filtered through a 0.22 μm PVDF membrane prior to FTICR-MS measurements.

FTICR-MS measurement. All samples were measured by the FTICR-MS instrument equipped with a 9.4 T superconducting magnet system (Solarix XR, Bruker) and electrospray ionization (negative ion mode, -ESI) at Tohoku University, Sendai, Japan. All FTICR-MS spectra were measured with the following instrumental conditions: -4.5 kV capillary voltage; 150 μL/h direct infusion rate; 2 megaword time-domain data size; 450 average scans; 1 ms ion accumulation; 150 -1,500 mass-to-charge ratio (m/z) range, and > 200, 000 resolving power (m/z= 399). Parent ions for the Treatment D at nine nominal masses (267, 311, 373, 407, 445, 477, 485, 559, and 6230 were isolated at 1 Da mass windows and fragmented in the quadrupole using the collision-induced dissociation by argon gas. The fragmentation spectra were recorded in the same FTCR MS instrument with 100 average scans and 2 megaword time-domain data size. The collision voltage and ion accumulation time were adjusted to obtain optimal fragmentation spectra (Table S1). Prior to the measurement, the FTICR-MS instrument was rinsed by the deuterated solvent (MeOD + D_2O) for D-SRNOM sample and normal solvent (MeOH + H_2O) for the other samples to prevent the possible exchange of H/D between DOM molecules and residual solvents in the instrument [18]. All FTICR-MS and FTICR-MS/MS spectra were externally calibrated with ion clusters using the NaI solution before measurement and internally recalibrated with known CHO-homologous series

174 of freshwater DOM to achieve a mass accuracy < 1.0 ppm for the entire spectrum during post-data
175 processing [12,40].

176 **Algorithm description.** The FTMSDeu algorithm was developed based on our previous
177 NOMDBP Code [40] by incorporating D in the formula assignment and extending the formula
178 assignment capability to Cl- and Br-free solutions containing I (referred to as Org-I_n hereafter).
179 The FTMSDeu algorithm is executed with the flow depicted in Figure 1. Briefly, after inputting a
180 calibrated UHR-MS spectral information (*m*/*z*, intensity, signal-to-noise ratio [*S*/*N*]), all
181 chemically possible solutions are calculated for each *m*/*z* according to following calculation
182 conditions: *i.e.*, (i) mass error tolerance (typically 1.0 ppm), (ii) maximum number of element, (iii)
183 maximum number of D, (iv) DBE minus O rule [12], and (v) nitrogen rule. Then, unlikely solutions
184 are filtered based on the ^{13}C-isotopic pattern with the acceptable intensity error tolerance (30 %
185 relative to the theoretical value). For a given *m*/*z*, if all filtered solutions are halogen-free, then the
186 optimum solution is selected in the first scenario (typically suitable for NOM) with the precedence
187 of (i) minimum number of N+S+P, (ii) minimum number of S+P, (iii) D≤O rule (optional rule only
188 for D-labeled UHR-MS spectra), and (iv) minimum error. Otherwise, all filtered solutions are
189 inspected in the second scenario, where organohalogen formulae containing non-oxygen
190 heteroatoms must have sufficient intensity (*e.g.*, $S/N \geqslant 10$), and Org-I_n formulae must be restricted
191 to *m*/*z* in the range from its nominal value minus 0.4 to plus 0.02 (namely the empirical I_n-DBPs
192 mass distribution rule). Then, the effective candidates of organohalogen formula are determined
193 including (i) Org-I_n, (ii) organohalogen formulae solely containing single Cl or Br (Org-Cl_1 or
194 Org-Br_1), and (iii) organohalogen formulae with multiple numbers of Cl+Br using our previously
195 proposed rules (*i.e.*, precursor and new peak appearance inspection [40] and Cl and Br isotopic
196 pattern validation). The optimum formula for this given *m*/*z* among non-halogen and

organohalogen formulae is subsequently selected with the priority of (i) maximum number of Cl+Br (only for organohalogen candidates with multiple numbers of Cl+Br), (ii) minimum number of N+S+P, (iii) minimum number of S+P, and (iv) minimum error [40]. Once all monoisotopic peaks are assigned to unequivocal formulae, all unassigned peaks and assigned peaks in both scenarios are combined to assign isotopic formulae for ^{13}C, ^{18}O, ^{34}S, ^{37}Cl, and ^{81}Br based on their isotopic patterns of natural abundances with an acceptable intensity error of 30%. Some important molecular parameters (*e.g.* (H+D)/C, O/C, X/C, DBE, AI_{mod}, and NOSC) are also calculated and exported together with formula results.

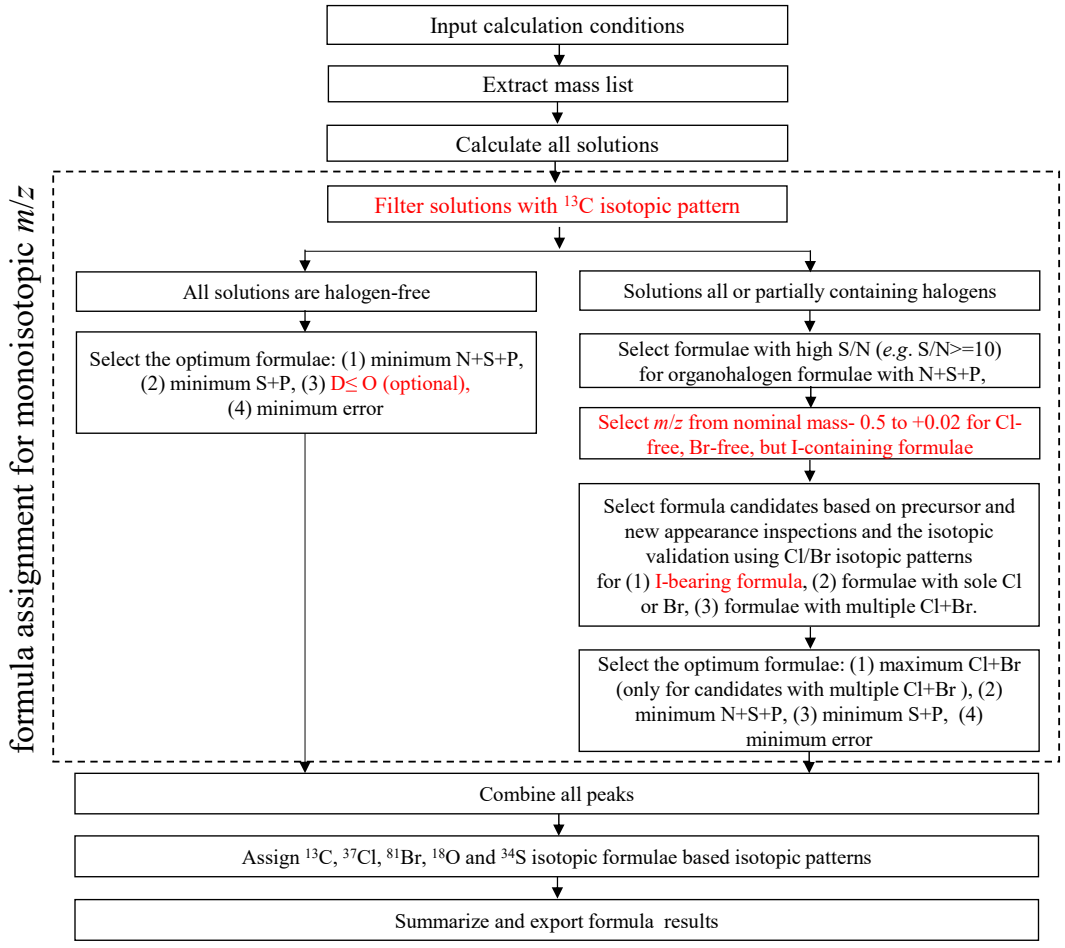

Figure 1. The FTMSDeu algorithm flow. Red words indicate new functions compared with our previous NOMDBP Code[40].

It is worth noting that some false positive solutions can be caused by the incorporation of D for Org-X_n formula assignment due to the close mass difference of $C_2H_3O_4$ versus D_6Br_1 ($\Delta m/z$= 0.18 mDa), $C_4H_3O_5$ versus $D_5N_3Br_1$ ($\Delta m/z$= 0.02 mDa), C_1D_3 versus $^{13}C_1H_5$ ($\Delta m/z$ = 0.17 mDa), and C_4D_{10} versus $H_{20}O_3$ ($\Delta m/z$= 0.22 mDa). For example, peaks at m/z= 306.945864 and 307.952127 have multiple Org-X_n solutions within 1.0 ppm mass error ($C_9H_9O_7Br_1$ versus $C_7H_6D_6O_3Br_2$ and $C_9H_8D_1O_7Br_1$ versus $C_7H_5D_7O_3Br_2$, respectively). However, due to the obviously different isotopic patterns for the Org-Br_1 and Org-Br_2 formulae, as exemplified in Figure S2, the true positive formulae (*i.e.*, $C_9H_9O_7Br_1$, and $C_9H_8D_1O_7Br_1$) can be assigned to m/z 306.945864 and 307.952127, respectively. The isotopic pattern (in this case for Br) is, therefore, an effective tool to solve the formula assignment issue of $C_2H_3O_4$ versus D_6Br_1. Analogously, for m/z= 313.056496, the candicate formula $C_9H_{11}D_5O_4N_3Br_1$ can be declined due to the absence of ^{81}Br isotopic peak in the identical UHR-MS spectrum (Figure S3), and the true positive formula, $C_{13}H_{14}O_9$ can be ultimately assigned, which is further validated by the minor error (3%) for intensity ratio between measured intensity ratio of ^{13}C isotope and its theoretical value.

The utilization of ^{13}C isotopic pattern can also solve the formula assignment issue of C_1D_3 versus $^{13}C_1H_5$, when the monoisotopic peaks have sufficiently high intensity. For example, if $^{13}C_1C_{19}H_7D_7O_5$ was assigned for m/z= 341.124221 (RA=7.59%) in the UHR-MS spectrum of D-SRNOM, there must be a distinct monoisotopic peak at m/z= 340.1207855 with a theoretical relative abundance (RA) of 35.09% (Figure S4). This formula is, therefore, found to be a false positive solution for m/z= 341.124221. However, there are still two candidate formulae without non-oxygen heteroatom $C_{20}H_2D_{10}O_5$, and $C_{16}H_{22}O_8$ calculated for this ion (*i.e.*, C_4D_{10} versus $H_{20}O_3$). The carboxylic and hydroxylic functional groups (-COOH and -OH) are the major moieties containing labile H in NOM molecules[13], suggesting that the number of D in NOM

231 molecules is less than the number of O under the D_2O system. Also, the hydroxylation (*e.g.*, UV
232 irradiation treatment) can be important mechanism that incorporates labile or non-labile OH into
233 aromatic molecules [45-47], and the number of D becomes less than O number for NOM molecules
234 under the hydroxylation with D_2O. Therefore, the D ≤ O rule (D number ≤ O number) is
235 incorporated in the FTMSDeu algorithm to assign formulae for D-labeled UHR-MS spectra of
236 NOM. By introducing the D ≤ O rule, the true positive formula, $C_{16}H_{22}O_8$, is finally assigned to
237 *m*/*z*= 341.124221. The D≤ O rule is also supported by the fact that NOM is rich in refractory
238 carboxyl-rich alicyclic molecules (CRAM) with the compositional space of DBE/C = 0.30- 0.68,
239 DBE/H = 0.20- 0.95, and DBE/O = 0.77- 1.75 [21]. For *m*/*z*= 341.124221, $C_{20}H_2D_{10}O_5$ is far from
240 the restricted area of CRAM, while $C_{16}H_{22}O_8$ (DBE/C=0.38, DBE/H=0.28, and DBE/O=0.75) is
241 close to its empirical area border. A formula assignment flow was exemplified in Figure S5 for the
242 FTICR-MS spectra for Treatment B, D-SRNOM in D_2O, and Treatment D (the parent ions at *m*/*z*=
243 306.945864, 341.121157, and 432.942712, respectively).

244 **Data analysis**. Formula assignment was conducted by the FTMSDeu algorithm using the
245 following calculation conditions: *S*/*N* ≥ 6 and ≥ 10 for non-halogenated and halogenated
246 monoisotopic formula, respectively; 0.3 ≤ (H+Cl+Br+I)/C ≤ 2.25 and 0 < O/C ≤ 1.2 for molecule
247 with C ≥ 5, (H+Cl+Br+I)/C ≤ 4 and 0 ≤ O/C ≤ 1.2 for molecule with C ≤ 4; an integer value ≥ 0
248 for double bond equivalent (DBE); 1≤ ^{12}C ≤ 50; 0 ≤ D ≤ 10 for chlorinated or non-chlorinated
249 SRNOM in D_2O and D = 0 for H-SRNOM; ^{13}C ≤ 2; ^{18}O ≤ 1; -10 ≤ DBE-O ≤ 10; ^{14}N ≤ 5; ^{32}S ≤ 3;
250 ^{33}S ≤ 1; P ≤ 1; ^{35}Cl ≤ 5; ^{37}Cl ≤ 5; ^{79}Br ≤ 5; ^{81}Br ≤ 5; and I=0 and ≤ 5 for all chlorinated treatments
251 without and with I^-, respectively. One H was assumed to be lost during the negative ESI process
252 for all treatments, expect for D-SRNOM, in which one D was lost. Thus, one H or D was added to
253 calculate the neutral formula for the relevant samples. The assigned formulae were classified into

eight biochemical groups in the van Krevelen diagram based on the reported criteria [40]. X_n-DBPs precursor herein was defined as the molecule or molecule moiety that forms X_n-DBPs via electrophilic substitution and/or electrophilic addition. The precursor of a given X_n-DBPs formula ($C_xH_yO_zD_kX_l$) was estimated as $C_xH_{y+l-k}O_{z-k}$ according to stoichiometric changes of electrophilic substitution and electrophilic addition. The relative contribution of electrophilic substitution and electrophilic addition for a given X_n-DBPs molecule ($Cont_{Sub1}$ and $Cont_{Add1}$, respectively) and all X_n-DBPs molecules ($Cont_{Sub2}$ and $Cont_{Add2}$, respectively) were quantified by Eqs. (S1)-(S4) in Content S1. The DBE, modified aromaticity index (AI_{mod}), the nominal oxidation state of carbon (NOSC), and the intensity-weighted values of molecular parameters were calculated with Eqs. (S5)-(S8) in Content S2. The homologous series of all I_n-DBPs were also inspected with an in-house algorithm based on (i) I_n-DBPs formulae validated by FTICR-MS/MS, (ii) common NOM formula building blocks (*i.e.*, H_2, H_2O, C, CH_2, CO_2, and CO), and (iii) building blocks representing electrophilic substitution of iodination (*i.e.*, mass of I minus H, I-H) and electrophilic addition of iodination (*i.e.*, mass of I plus H, I+H). The network diagram was visualized by Gephi software. Principal component analysis (PCA) was conducted with MATLAB using the molecular parameters tabulated in Table S2.

RESULTS AND DISCUSSION

Labile H in SRNOM. While H-SRNOM and D-SRNOM samples shared a similar spectral profile in the overall UHR-MS spectra (Figure S6A), the spectrum for D-SRNOM was more complicated than that for H-SRNOM due to deuteration of labile H in SRNOM molecules. The discrepancy of peak intensity was more apparent for D-SRNOM at even nominal masses than that for odd nominal mass. H-SRNOM peaks at the even nominal masses had lower intensities than

277 those for D-SRNOM (Figures S6B and S6C). The former peaks were attributed mostly to the ^{13}C-
278 isotopologues and to lesser extent to the compounds containing even number of N, while the higher
279 intensity of latter peak was assigned to peaks for deuterated compounds with an odd number of D.
280 Consistent with the previous observation [13], the presence of multiple numbers of labile H in
281 SRNOM (Figure S7) resulted in about twofold increase in the number of assigned peaks for D-
282 SRNOM compared to that for H-SRNOM with 2 to 6 number of labile H (Figure S8).

283 Nonetheless, it is noteworthy that, during negative-ESI ionization, a few D-SRNOM
284 molecules that have lost one labile H are hard to be distinguished from more abundant D-SRNOM
285 molecules and are considered as molecules lossing one labile D for the number estimation of liable
286 D. This was also supported by the relatively small intensity (10%) of molecules that have mostly
287 lost one labile D during negative-ESI ionization (Figure S8). Lignin-like and tannic-like
288 compounds accounted for 67.7% and 28.5% of D-SRNOM molecules, respectively, and generally
289 had more labile D than other types of D-SRNOM molecules (Figure S9). The number of labile D
290 linearly increased with increasing average values of O number and O/C ratios for D-SRNOM
291 molecules (R^2=0.944 and 0.968, respectively, Figure S10). This result further supported the
292 hypothesis that carboxyl and hydroxyl functional groups were the predominant contributors of
293 labile H (or D) for SRNOM [16-18]. Furthermore, Figure S10A revealed the presence of O-containing
294 function groups irrelevant to labile H (such as the carbonyl or ether group) [13] for D-SRNOM
295 molecules with number of labile D being no more than seven.

296 **Identification of I_n-DBPs**. Regarding I-containing compounds, 1,436 unequivocal I_n-DBPs
297 formulae were identified by our FTMSDeu algorithm for the Treatment D. Also, unique Cl_mI_n-
298 DBPs was also detected and validated with the Cl isotopic pattern ($C_2H_3O_2Cl_1I_2$ in Figure S11). In
299 the FTICR-MS/MS spectra of parent ions at nine selected nominal masses, the distinct I^- peak at

300 *m*/*z*=126.9050165 was detected, confirming the presence of organo-iodine compounds in these
301 nominal masses (Table S1) [48,49]. Fragment ions with neutral losses of I radical (I·, 126.904468 Da)
302 and HI (127.912293 Da) were also identified in these FTICR-MS/MS spectra (mass error tolerance
303 <1.0 ppm, Table S1, and Figure S12). For example, nearly all parent ions with low *m*/*z* (*e.g.*, <
304 560) had lost a single or multiple numbers of I·or HI.

305 There were 411 nodes and 388 edges identified in the homologous series inspection of all I_n-
306 DBPs in the Treatment D, revealing that 411 unique I_n-DBPs compounds had direct homologous
307 connections to FTICR-MS/MS-validated I_n-DBPs formulae. As exemplified in Figure S13,
308 another 13 I_n-DBPs formulae were supported by $C_7H_4O_2I_2$, which was validated by FTICR-
309 MS/MS, and typical blocks including CO_2, H_2O, CO, C, CH_2, and +I-H. Furthermore, 178
310 unequivocal I_n-DBPs were computed under the calculation conditions. Totally, 589 I_n-DBPs
311 compounds identified in the aforementioned two scenarios were considered to be highly reliable
312 and accounted for 41.0% and 59.2% of the total number and intensities, respectively, for all 1,436
313 assigned I_n-DBPs formulae in the Treatment D. The equivocal solutions for 300 other peaks were
314 caused by the close mass differences of H_4I_1 versus $C_3O_2S_1P_1$ and H_4I_1 versus $C_4O_1S_1{}^{35}Cl_1$
315 ($\Delta m/z$=0.11 and 0.07 mDa, respectively). However, the solutions of $C_3O_2S_1P_1$ and $C_4O_1S_1{}^{35}Cl_1$
316 were rejected in our algorithm as a result of (i) the absence of detectable ^{37}Cl-isotopic peaks if
317 presence [40], (ii) deficiency of non-oxygen heteroatom in NOM precursors [29] and (iii) the selected
318 I_n-DBPs formula having more moderate degree of saturation than $C_3O_2S_1P_1$-containing solution.
319 For example, the non-oxygen heteroatom-free I_n-DBPs formula, $C_9H_9O_7I_1$ with moderate degree
320 of saturation (DBE=5), was attributed to peak at *m*/*z* 354.932139 rather than the non-oxygen
321 heteroatom-containing unsaturated formulae $C_{13}H_5O_8S_1Cl_1$ and $C_{12}H_5O_9S_1P_1$ (DBE=11). For
322 similar reason, I_n-DBPs formulae with a minimum number of non-oxygen heteroatom were

assigned to the other 547 peaks, and most of them (>91%) had *m*/*z* values >500. Therefore, in addition to relabile Cl_n-DBPs and Br_n-DBPs formulae, our FTMSDeu algorithm can automatically assign I_n-DBPs formulae with high accuracy, providing an useful tool for non-targeted screen of halogenated organic compounds in the complex organic mixtures.

The enlarged UHR-MS spectrum in Figure 2 indicated the applicability of the I_n-DBPs mass distribution rule (*i.e.*, I_n-DBPs ions locate in the mass window of nominal value minus 0.4 to plus 0.02) due to the significant mass deficiency of ^{127}I isotope compared with its nominal mass (126.904468-127=-0.095532) and the mass window of NOM ions from nominal value to nominal value plus 0.3. It should be noted that some I_n-DBPs formula containing non-oxygen heteroatoms such as sulfur and nitrogen (namely, CHOSI and CHONI, respectively) were identified in the UHR-MS spectrum for the treatment D. The typical CHOSI ($C_2H_1O_3S_1I_3$) was detected at *m*/*z* 484.670894 (Figure 2) and was confirmed to contain sulfo group (Figure S12D) which can be attributed to sulfotriiodoethylene. Sulfur-bearing X_n-DBPs has been proposed to be generated by the bromination of surfactant degradation products in seawater [50] and wastewater [51], and chlorination of CHOS compounds in secondary effluent [52]. Because of the low abundance of CHOS molecules in SRNOM (6.5% of total intensity), CHOSI species herein can be generated by the reaction with dehalogenation agent (Na_2SO_3) used to terminate the chlorination. Analogous to halomethane ions (*e.g.* $[CHBr_2]^-$ and $[CHClBr_2]^-$ detected in the Treatment B [40]), the newly discovered oxygen-free $[C_3N_2I_3]^-$ ion in Figure 2 (which was validated by FTICR-MS/MS, Table S1) is unlikely to be ionized in negative ESI mode and therefore this molecule is most likely generated by the dissociation of $C_3N_2I_3$ moiety from the large parent CHONI molecule during ionization process in ESI section [40].

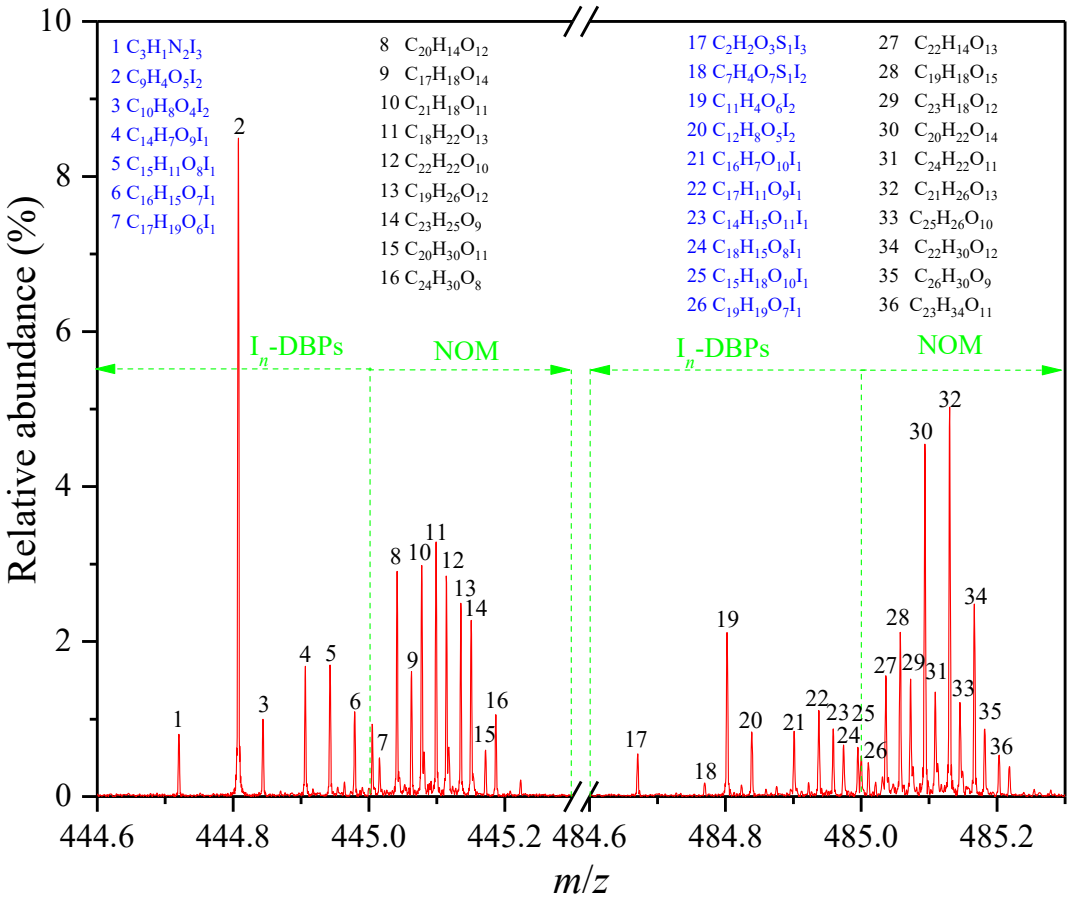

345

346 **Figure 2.** The enlarged UHR-MS spectrum for the Treatment D at the nominal masses of 445

347 and 485.

348 **Characteristics of X_n-DBPs formed in the D_2O system**. As illustrated in Figure 3, the

349 deuterated X_n-DBPs species were detected with high resolution by the FTICR-MS technique. The

350 measured UHR-MS spectra for deuterated and non-deuterated DBPs species containing Cl and/or

351 Br were highly close to their theoretical spectra (Figures 3, S14 and S15), suggesting the high

352 accuracy of our FTMSDeu algorithm in assigning both deuterated and non-deuterated X_n-DBPs

353 formulae. The FTMSDeu algorithm had identified 1,573, 1,025, and 1,623 unique X_n-DBPs

354 species in Treatments A, B, and C, respectively. Compared to Cl_n-DBPs, Br- or I- containing X_n-

355 DBPs species tended to be deuterated during the disinfection process, suggesting that electrophilic

addition contributed to larger extent in the formation of Br- or I-bearing X_n-DBPs species than electrophilic substitution. HOCl could readily oxidize Br^- and I^- to HOBr (which is more reactive with NOM molecules)[53], and thermodynamically unstable HOI ($5HOI = 2I_2 + IO_3^- + H^+ + 2H_2O$, which is less likely to participate in X_n-DBPs formation)[54], respectively. Therefore, Br_n-DBPs and Cl_n-DBPs were observed to be the predominant X_n-DBPs species (accounting for 74.5% and 94.6% of all DBPs species in Treatments B and C, respectively, Figure S16). The formula number and intensity for Br_n-DBPs were substantially larger than those for Cl_n-DBPs in Treatment B (Figure S16), suggesting that Br_n-DBPs are effectively formed via oxidation of Br^- by active chlorine species followed by reactions of HBrO with DOM molecules. Unlike our previous results which showed that more X_n-DBPs was yielded in the SRNOM+ClO^-+Br^- treatment than the SRNOM+ClO^- treatment [40], the proportion of total X_n-DBPs intensity in Treatment B of this study was approximately 80% of that in Treatment A. This discrepancy could be related to different initial solution pH values (8.9 and 7.5 in this and previous study, respectively). As an effective disinfectant, ClO^- is the predominant chlorine species in Treatment B, but this Cl form is six orders of magnitude less reactive with Br^- compared to HClO, yielding BrO^- at a much slower rate for Br_n-DBPs formation [25]. X_1-DBPs and X_2-DBPs compounds were the dominant X_n-DBPs species in all three treatments (Figure S17) due to the passivating effect of halogen atom for successive reception of halogen atoms during X_n-DBPs formation [55]. Furthermore, X_n-DBPs species could be well distinguished by PCA analysis with three components (Figure S18) using the intensity-weighted molecular parameters tabulated in Table S2. The Br_n-DBPs and Cl_mI_n-DBPs in Treatments B and C were separated from other X_n-DBPs species by principle component 1, which was related to the intensity-weighted number of carbon (C_{iw}). Principle component 3 associated

with the degree of unsaturation and number of D was capable of differentiating Cl_n-DBPs in Treatment A and Treatment C from others.

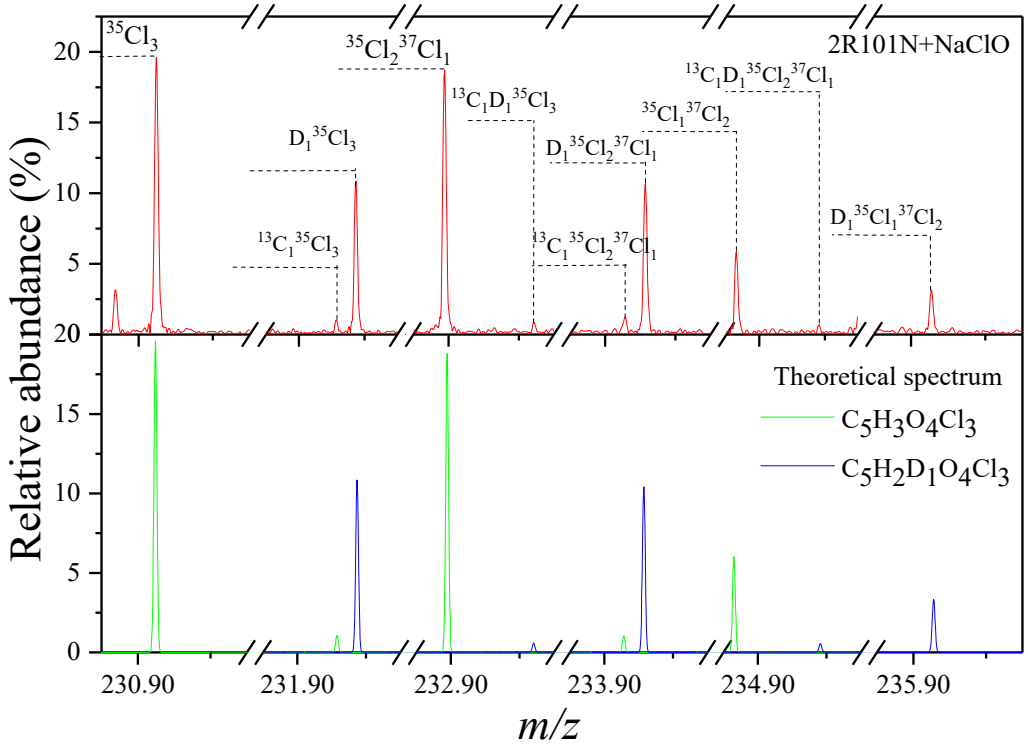

Figure 3. Representative measured and theoretical UHR-MS spectra of $C_5H_3O_4Cl_3$ and $C_5H_2D_1O_4Cl_3$. The measured UHR-MS spectrum for Treatment A.

Relative contribution for X_n-DBPs formation. The relative contributions of electrophilic addition and electrophilic substitution to X_n-DBPs formation in all treatments were calculated based on the intensity of all identified X_n-DBPs formulae (Table 1). Consequently, the electrophilic substitution was estimated to be the predominant mechanism for Cl_n-DBPs formation in Treatments A-C, contributing to 81.8% - 98.4% of Cl_n-DBPs formation, while the occurrence of HClO addition on unsaturated moieties of DOM molecules were less likely under the conditions examined due to the relatively lower rate of this pathway [28]. The PCA result also supported that Cl_n-DBPs showed higher degree of unsaturation and fewer number of D than the other X_n-DBPs

391 species (Figure S19). Compared to Cl_n-DBPs, the relative contribution of electrophilic addition
392 increased by approximately 20% for Br-containing X_n-DBPs species (Br_n-DBPs and Cl_mBr_n-DBPs,
393 see Treatment B in Table 1), but electrophilic substitution was still the major contributor in Br-
394 containing X_n-DBPs formation. In contrast, electrophilic addition played more critical roles in I-
395 containing X_n-DBPs species (I_n-DBPs and Cl_mI_n-DBPs accounting for 56.7% and 55.2%,
396 respectively) formation than electrophilic substitution. The increasing in the relative contribution
397 of electrophilic addition for Cl_n-DBPs, Br_n-DBPs, and I_n-DBPs is consistent with the increase in
398 the dissociation constants of hypohalous acid (Figure 4, R^2=0.90, p<0.05, note that pK_a are 7.50,
399 8.63 and 10.4 for HClO, HBrO, and HIO, respectively [25,56]) and decrease in the electronegativity
400 of halogens (Figure 4, R^2=0.82, p<0.05, electronegativity are 3.16, 2.96, 2.66, and 3.51 for Cl, Br,
401 I, and O, respectively). This observation was supported by the proposed reaction steps of
402 electrophilic addition, where X^+ atom in hypohalous acid initially transferred to the unsaturated
403 carbon bound to provide a halonium ion, forming transitional halohydrin products, followed by
404 subsequent addition of remaining OH^- [25,28]. The lower halogen electronegativity is favorable for
405 halohydrin formation, and consequently formed X_n-DBPs more via electrophilic addition. Moreover,
406 OCl^-, OBr^- and HOI were the initially dominant hypohalous acid species (80.3% , 66.6%, and
407 99.8%, respectively) under the condition examined (Figure S19). Therefore, the electrophilic
408 addition potential of HXO could be in order of HIO > HBrO > HClO, suggesting that reaction
409 pathways were determined by the halogen electrogenativity and acidity of reactive hypohalous
410 acid species. Furthermore, the contribution of electrophilic addition for X_n-DBPs species is
411 consistent with their degree of toxicity: *i.e.*, I_n-DBPs > Br_n-DBPs > Cl_n-DBPs [57]. This finding
412 highlights the importance of electrophilic addition in terms of formation of toxic X_n-DBPs species.
413

414 **Table 1**. The relative contribution of electrophilic addition and electrophilic substitution to
415 X_n-DBPs formation in different treatments.

Treatment	X_n-DBPs Species	X_n-DBPs Peaks	Relative Contribution (%)	
			Electrophilic Addition	Electrophilic Substitution
Treatment A (D_2O+ClO^-)	Cl_n-DBPs	4223	1.6	98.4
	Overall	**4223**	**1.6**	**98.4**
Treatment B (D_2O+ClO^-+Br^-)	Cl_n-DBPs	260	18.2	81.8
	Br_n-DBPs	2051	11.2	88.7
	Cl_mBr_n-DBP	309	28.8	71.2
	Overall	**2620**	**12.9**	**87.1**
Treatment C (D_2O+ClO^-+I^-)	Cl_n-DBPs	3544	1.5	97.6
	Cl_mI_n-DBPs	44	55.2	44.8
	I_n-DBPs	73	56.7	43.4
	Overall	**3661**	**3.1**	**96.9**

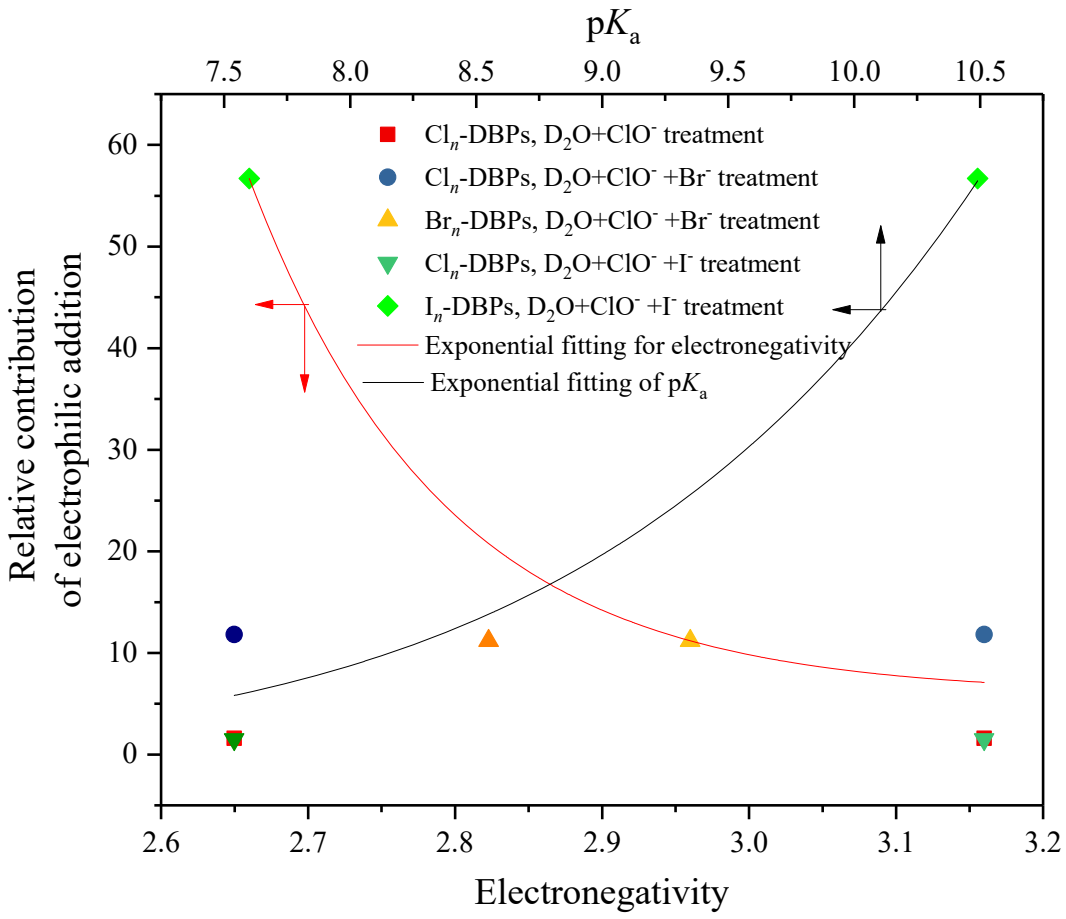

416

Figure 4. Relationship between relative contributions of electrophilic addition for Cl_n-DBPs, Br_n-DBPs, and I_n-DBPs and pK_a values of HOCl, HOBr, and HOI, respectively.

X_n-DBPs precursors. Putative precursors of X_n-DBPs compounds were determined by assuming that X_n-DBPs was formed via electrophilic addition and substitution reactions. In the calculation, only stoichiometric changes associated with electrophilic reactions (but not secondary reactions) were considered. Similar profiles were observed for van Krevelen diagram from three treatment conditions (*i.e.*, Treatments A-C, Figures 5A-5C), suggesting that the majority of X_n-DBPs compounds were derived from the halogenation of similar NOM precursors (Figure 5D) with active hypohalous acid species. Treatments A and C shared 1,622 X_n-DBPs (84.5% and 89.5% number of all X_n-DBPs species, respectively) and 930 X_n-DBPs precursors (88.9% and 87.9% number of total X_n-DBPs precursors, respectively). This result combined with van Krevelen diagram profile generally indicates that the majority of X_n-DBPs was originated from the electrophilic substitution of reactive chlorine with lignins- and tannins-like DOMs molecules with O/C=0.4-0.9 and H/C=0.5-1.5. Since the electrophilic substitution is dominant for Cl_n-DBPs in Treatments A and C (the contributions were to more than 97%), it can be reasonable to visually characterize Cl_n-DBPs precursors by replacing H/C with (H + Cl)/C in the van Krevelen diagram of chlorinated waters containing low concentrations of Br^- (*e.g.*, fresh groundwater) [40]. The ploted molecules on the *y*-axis (*i.e.*, O/C = 0) could be either X_n-DBPs species where halogen was electrophilically added to oxygen-free NOM molecules (*e.g.*, $C_3H_1D_1O_1Cl_3$, $C_4H_3D_2O_2Br_2$, and $C_8H_2D_2O_2Cl_1I_1$ in Treatments A, B, and C, respectively) or electrophilically substituted oxygen-free X_n-DBPs species (*e.g.*, halomethane in the Treatment B). Putative N-containing precursors were only identified in the Treatments B and C (Figure S20A) and were responsible for more toxic N-containing X_n-DBPs species than N-free X_n-DBPs compounds [26]. Putative precursors were

sometime not detected in some treatments (Figure S20B and Table S3), which could be due to the secondary reactions including oxidation and hydrolysis of electrophilically added and/or substituted X_n-DBPs species [26] and thus considered as putative precursor moieties for secondary X_n-DBPs formation. The fact that 613 X_n-DBPs precursors were identified in all three treatments suggests that non-selectivity of NOM molecules toward different reactive hypohalous acid species in X_n-DBPs formation. Moreover, considerable proportions (32.0%-55.0%) of putative precursors were involved in formation of multiple (different) unique X_n-DBPs species in the three treatments (Figure S20C), suggesting that the formation of X_n-DBPs is highly complex and diverse even when originating from the same NOM molecule. Compared to Treatment A, more unsaturated hydrocarbon and unsaturated lignins-like precursors were exclusively scattered in the left area of van Krevelen diagrams (O/C=0-0.3 and H/C=0.3-1.5) for the other two treatments. These precursors are not preferentially removed by typical treatments such as granular activated carbon adsorption and metal coagulation [58,59] in drinking water treatment and are responsible for formation of more toxic Br_n-DBPs and I_n-DBPs [57], highlighting the necessity of removing these precursors in drinking water systems.

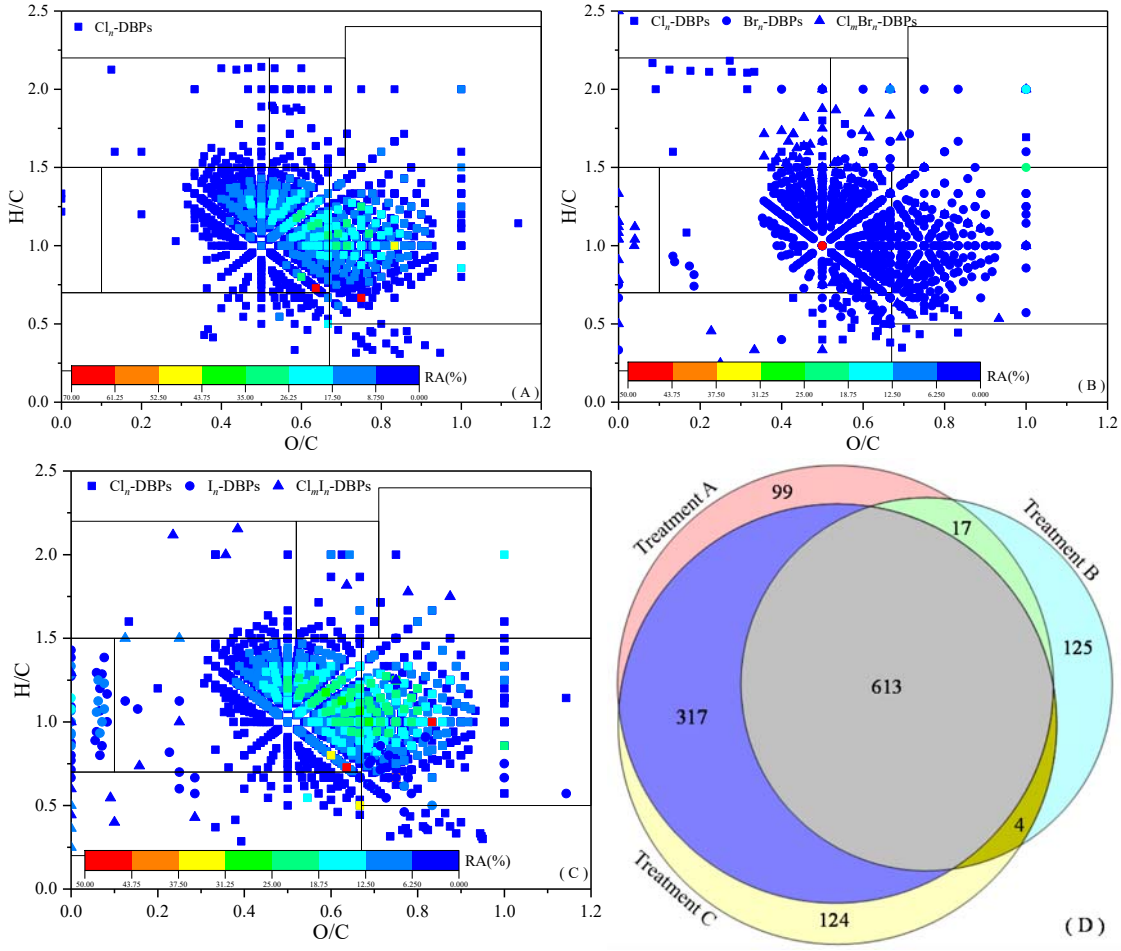

Figure 5. The van Krevelen diagrams of estimated X_n-DBPs precursors for Treatment A (A), Treatment B (B), and Treatment C (C); and the Venn diagram of all estimated unique X_n-DBPs precursors (D). RA(%) is the relative abundance of X_n-DBPs monoisotopic peaks.

Limits and Future direction

The main limitation of this study is the spontaneous exchange between -OD added to the backbone structure of NOM (as the backbone structure) and surrounding H_2O molecule during SPE extraction process. Such loss of D during the post-treatment (in case D_2O is not used for all the chemicals used) potentially underestimate the contribution of electrophilic addition to X_n-DBPs formation. The electrophilical addion of -OD to backbone structures will increase their

saturation degree, yielding less labile -OD than that with higher degree of unsaturation (*i.e.*, phenolic -OD). Moreover, given that OCl^-, OBr^-, and HOI are dominant active hypohalous acid species at the initial pH employed, this issue may be minor for Treatment A but non-negligible for Treatment C because H/D exchange in skeleton generally occurs in the presence catalysis (or under high temperature) [19]. This issue, however, can be satisfactorily solved by using D-^{18}O dual-isotope labeling, where D and ^{18}O are added in precursors together with halide atoms for electrophilic addition, and only halide atoms substitute with H atoms in precursors for electrophilic substitution. X_n-DBPs electrophilically added in the aromatic skeleton are characterized by identical numbers of ^{18}O and halide atoms; and X_n-DBPs electrophilically added in unsaturated side chains contain identical numbers of D, ^{18}O, and halide atoms. Thus, UHR-MS techniques coupled with D/^{18}O isotope labeling could be useful in elucidating X_n-DBPs formation mechanisms. At the same time, further updates of our FTMSDeu algorithm are necessary for UHR-MS spectra labeled with ^{18}O, ^{13}C, and other isotopes with development of associated new filtering rules. For example, both $C_8H_8O_5Cl_2$ and $C_7H_6O_3{}^{18}O_1N_2Cl_2$ are within the 1.0 ppm mass error tolerance for the peak at m/z =252.967559 due to the close mass difference between CH_2O_2 and $N_2{}^{18}O_1$ ($\Delta m/z$= 0.17 mDa).

CONCLUSIONS

In this study, for the first time, the FTMSDeu algorithm was successfully developed for D-labeled UHR-MS spectra and employed to automatically assign chemical formulae for organoiodine (filtered with newly proposed I_n-DBPs mass distribution rule), organochlorine, and organobromine. Its assignment accuracy for organo-iodine compounds was further validated with FTICR-MS/MS technique and homologous-based network analysis. It was found that the number of labile D in SRNOM molecules linearly increased with their O content and O/C ratios, suggesting

that labile D is attributed to the O-containing active functional groups (*e.g.*, -COOH and -OH). The relative contributions of electrophilic addition and substitution were dependent on the halogen species involved in the reactions, and the solution pH and pK_a values for hypohalous acids, as well as type of halogen, could be important parameters. Under the conditions examined in this study, the electrophilic substitution was the predominant mechanism for Cl_n-DBPs and Br-containing X_n-DBPs, while electrophilic addition becomes significant in the formation I-containing X_n-DBPs. The secondary reactions of electrophilically added and/or substituted X_n-DBPs species were indirectly supported by few putative precursor moieties. The UHR-MS technique coupled with isotope labeling was of significant importance in revealing the transformation of DOM in natural and engineered systems such as water and wastewater treatments. Overall, our FTMSDeu algorithm has laid valuable basis for further developing formula assignment for UHR-MS spectra labeled with the other isotopes.

ASSOCIATED CONTENT

Supporting Information

Calculation of contribution and intensity weighted DBE, AI_{mod} and NOSC; FTICR-MS/MS spectra and ions; molecular parameters for PCA analysis; commonly estimated X_n-DBPs precursors; representative measured and theoretical UHR-MS spectra; broadband and expended UHR-MS spectra; relative intensity percentage of D-SRNOM molecules; Van Krevelen diagrams; Relationship between labile D number and average oxygen number and O/C; network plot for $C_7H_4O_2I_2$; unique formula number, intensity proportions, PCA results of all X_n-DBPs; Speciation distribution of hypohalous acid.

ACKNOWLEDGEMENTS

This study was financially supported by the Japan Society for the Promotion of Science (NO. 17H04588, 19H02271), the Special Funding for Discipline Construction from China University of Geosciences (NO. 162301212611) and the National Natural Science Foundation of China (No. 42107484). The authors appreciate the technical support from Hiroyuki Momma in FTICR-MS measurement.

REFERENCES

(1) Kostyukevich, Y.; Kononikhin, A.; Zherebker, A.; Popov, I.; Perminova, I.; Nikolaev, E. *Anal. Bioanal. Chem.* **2014**, *406*, 6655-6664.
(2) Zhang, X.; Han, J.; Zhang, X.; Shen, J.; Chen, Z.; Chu, W.; Kang, J.; Zhao, S.; Zhou, Y. *Chemosphere* **2020**, *260*, 127458.
(3) Mopper, K.; Stubbins, A.; Ritchie, J. D.; Bialk, H. M.; Hatcher, P. G. *Chem. Rev.* **2007**, *107*, 419-442.
(4) Cooper, W. T.; Chanton, J. C.; D'Andrilli, J.; Hodgkins, S. B.; Podgorski, D. C.; Stenson, A. C.; Tfaily, M. M.; Wilson, R. M. *Mass Spectrom. Rev.* **2021**.
(5) Kim, S.; Kim, D.; Jung, M. J.; Kim, S. *Mass Spectrom. Rev.* **2021**.
(6) Fievre, A.; Solouki, T.; Marshall, A. G.; Cooper, W. T. *Energy Fuels* **1997**, *11*, 554-560.
(7) Kujawinski, E. B.; Behn, M. D. *Anal. Chem.* **2006**, *78*, 4363-4373.
(8) Tziotis, D.; Hertkorn, N.; Schmitt-Kopplin, P. *Eur. J. Mass Spectrom.* **2011**, *17*, 415-421.
(9) Tolić, N.; Liu, Y.; Liyu, A.; Shen, Y.; Tfaily, M. M.; Kujawinski, E. B.; Longnecker, K.; Kuo, L.-J.; Robinson, E. W.; Paša-Tolić, L.; Hess, N. J. *Anal. Chem.* **2017**, *89*, 12659-12665.
(10) Schum, S. K.; Brown, L. E.; Mazzoleni, L. R. *Environ. Res.* **2020**, *191*, 110114.
(11) Merder, J.; Freund, J. A.; Feudel, U.; Hansen, C. T.; Hawkes, J. A.; Jacob, B.; Klaproth, K.; Niggemann, J.; Noriega-Ortega, B. E.; Osterholz, H.; Rossel, P. E.; Seidel, M.; Singer, G.; Stubbins, A.; Waska, H.; Dittmar, T. *Anal. Chem.* **2020**, *92*, 6832-6838.
(12) Fu, Q. L.; Fujii, M.; Riedel, T. *Anal. Chim. Acta* **2020**, *1125*, 247-257.
(13) Kostyukevich, Y.; Kononikhin, A.; Popov, I.; Kharybin, O.; Perminova, I.; Konstantinov, A.; Nikolaev, E. *Anal. Chem.* **2013**, *85*, 11007-11013.
(14) Zherebker, A. Y.; Airapetyan, D.; Konstantinov, A. I.; Kostyukevich, Y. I.; Kononikhin, A. S.; Popov, I. A.; Zaitsev, K. V.; Nikolaev, E. N.; Perminova, I. V. *Analyst* **2015**, *140*, 4708-4719.
(15) Zherebker, A.; Kostyukevich, Y.; Kononikhin, A.; Kharybin, O.; Konstantinov, A. I.; Zaitsev, K. V.; Nikolaev, E.; Perminova, I. V. *Anal. Bioanal. Chem.* **2017**, *409*, 2477-2488.
(16) Zherebker, A.; Lechtenfeld, O. J.; Sarycheva, A.; Kostyukevich, Y.; Kharybin, O.; Fedoros, E. I.; Nikolaev, E. N. *Anal. Chem.* **2020**, *92*, 9032-9038.
(17) Zherebker, A.; Shirshin, E.; Rubekina, A.; Kharybin, O.; Kononikhin, A.; Kulikova, N. A.; Zaitsev, K. V.; Roznyatovsky, V. A.; Grishin, Y. K.; Perminova, I. V.; Nikolaev, E. N. *Environ. Sci. Technol.* **2020**, *54*, 2667-2677.
(18) Kostyukevich, Y.; Kononikhin, A.; Popov, I.; Nikolaev, E. *Anal. Chem.* **2013**, *85*, 5330-5334.

(19) Kostyukevich, Y.; Acter, T.; Zherebker, A.; Ahmed, A.; Kim, S.; Nikolaev, E. *Mass Spectrom. Rev.* **2018**, *37*, 811-853.
(20) Ritchie, J. D.; Perdue, E. M. *Geochim. Cosmochim. Acta* **2003**, *67*, 85-96.
(21) Hertkorn, N.; Benner, R.; Frommberger, M.; Schmitt-Kopplin, P.; Witt, M.; Kaiser, K.; Kettrup, A.; Hedges, J. I. *Geochim. Cosmochim. Acta* **2006**, *70*, 2990-3010.
(22) Liu, X. Y.; Chen, L.; Yang, M. T.; Tan, C. Q.; Chu, W. H. *Water Res.* **2020**, *184*.
(23) DeMarini, D. M. *Environ. Mol. Mutagen.* **2020**, *61*, 588-601.
(24) Powers, L.; Gonsior, M. *Curr. Opin. Environ. Sci. Health* **2019**, *7*, 52-60.
(25) Brezonik, P. L.; Arnold, W. A.; Oxford University Press, USA: New York, 2011.
(26) Sun, X. F.; Chen, M.; Wei, D.; Du, Y. G. *J. Environ. Sci.* **2019**, *81*, 52-67.
(27) Hao, Z. N.; Yin, Y. G.; Cao, D.; Liu, J. F. *Environ. Sci. Technol.* **2017**, *51*, 5464-5472.
(28) Deborde, M.; von Gunten, U. *Water Res.* **2008**, *42*, 13-51.
(29) Koch, B. P.; Dittmar, T.; Witt, M.; Kattner, G. *Anal. Chem.* **2007**, *79*, 1758-1763.
(30) Longnecker, K.; Kujawinski, E. B. *Rapid Commun. Mass Spectrom.* **2016**, *30*, 2388-2394.
(31) Stenson, A. C.; Marshall, A. G.; Cooper, W. T. *Anal. Chem.* **2003**, *75*, 1275-1284.
(32) Postigo, C.; Cojocariu, C. I.; Richardson, S. D.; Silcock, P. J.; Barcelo, D. *Anal. Bioanal. Chem.* **2016**, *408*, 3401-3411.
(33) Gonsior, M.; Schmitt-Kopplin, P.; Stavklint, H.; Richardson, S. D.; Hertkorn, N.; Bastviken, D. *Environ. Sci. Technol.* **2014**, *48*, 12714-12722.
(34) Zhang, H. F.; Zhang, Y. H.; Shi, Q.; Zheng, H. D.; Yang, M. *Environ. Sci. Technol.* **2014**, *48*, 3112-3119.
(35) Andersson, A.; Harir, M.; Gonsior, M.; Hertkorn, N.; Schmitt-Kopplin, P.; Kylin, H.; Karlsson, S.; Ashiq, M. J.; Lavonen, E.; Nilsson, K.; Pettersson, A.; Stavklint, H.; Bastviken, D. *Environ. Sci. Wat. Res. Technol.* **2019**, *5*, 861-872.
(36) Zhang, H. F.; Zhang, Y. H.; Shi, Q.; Hu, J. Y.; Chu, M. Q.; Yu, J. W.; Yang, M. *Environ. Sci. Technol.* **2012**, *46*, 4396-4402.
(37) Luek, J. L.; Schmitt-Kopplin, P.; Mouser, P. J.; Petty, W. T.; Richardson, S. D.; Gonsior, M. *Environ. Sci. Technol.* **2017**, *51*, 5377-5385.
(38) Luek, J. L.; Harir, M.; Schmitt-Kopplin, P.; Mouser, P. J.; Gonsior, M. *Water Res.* **2018**, *136*, 200-206.
(39) Gonsior, M.; Powers, L. C.; Williams, E.; Place, A.; Chen, F.; Ruf, A.; Hertkorn, N.; Schmitt-Kopplin, P. *Water Res.* **2019**, *155*, 300-309.
(40) Fu, Q. L.; Fujii, M.; Kwon, E. *Anal. Chem.* **2020**, *92*, 13989-13996.
(41) Hua, G. H.; Reckhow, D. A.; Kim, J. *Environ. Sci. Technol.* **2006**, *40*, 3050-3056.
(42) Zhang, H. F.; Yang, M. *Sci. Total Environ.* **2018**, *627*, 118-124.
(43) Wang, X.; Wang, J.; Zhang, Y. H.; Shi, Q.; Zhang, H. F.; Zhang, Y.; Yang, M. *Sci. Total Environ.* **2016**, *554*, 83-88.
(44) Dittmar, T.; Koch, B.; Hertkorn, N.; Kattner, G. *Limnol. Oceanogr. Meth.* **2008**, *6*, 230-235.
(45) Xiang, Y. Y.; Fang, J. Y.; Shang, C. *Water Res.* **2016**, *90*, 301-308.
(46) Van Buren, J.; Prasse, C.; Marron, E. L.; Skeel, B.; Sedlak, D. L. *Environ. Sci. Technol.* **2020**, *54*, 8352-8361.
(47) Wu, Z. H.; Fang, J. Y.; Xiang, Y. Y.; Shang, C.; Li, X. C.; Meng, F. G.; Yang, X. *Water Res.* **2016**, *104*, 272-282.
(48) Yang, Y. J.; Peng, Y. E.; Chang, Q.; Dan, C. H.; Guo, W.; Wang, Y. X. *Anal. Chem.* **2016**, *88*, 1275-1280.
(49) Peng, H.; Chen, C. L.; Cantin, J.; Saunders, D. M. V.; Sun, J. X.; Tang, S.; Codling, G.; Hecker, M.; Wiseman, S.; Jones, P. D.; Li, A.; Rockne, K. J.; Sturchio, N. C.; Cai, M. H.; Giesy, J. P. *Environ. Sci. Technol.* **2016**, *50*, 10097-10105.
(50) Powers, L. C.; Conway, A.; Mitchelmore, C. L.; Fleischacker, S. J.; Harir, M.; Westerman, D. C.; Croue, J. P.; Schmitt-Kopplin, P.; Richardson, S. D.; Gonsior, M. *Environ. Sci. Wat. Res. Technol.* **2020**, *6*, 2521-2541.

(51) Liberatore, H. K.; Westerman, D. C.; Allen, J. M.; Plewa, M. J.; Wagner, E. D.; McKenna, A. M.; Weisbrod, C. R.; McCord, J. P.; Liberatore, R. J.; Burnett, D. B.; Cizmas, L. H.; Richardson, S. D. *Environ. Sci. Technol.* **2020**, *54*, 9374-9386.
(52) Zhang, B.; Wang, X.; Fang, Z.; Wang, S.; Shan, C.; Wei, S.; Pan, B. *Water Res.* **2021**, 117158.
(53) Westerhoff, P.; Chao, P.; Mash, H. *Water Res.* **2004**, *38*, 1502-1513.
(54) Urbansky, E. T.; Cooper, B. T.; Margerum, D. W. *Inorg. Chem.* **1997**, *36*, 1338-1344.
(55) Hao, Z. N.; Shi, F. Q.; Cao, D.; Liu, J. F.; Jiang, G. B. *Environ. Sci. Technol.* **2020**, *54*, 1668-1676.
(56) Bichsel, Y.; von Gunten, U. *Water Res.* **2000**, *34*, 3197-3203.
(57) Dong, H. Y.; Qjang, Z. M.; Richardson, S. D. *Accounts Chem. Res.* **2019**, *52*, 896-905.
(58) Riedel, T.; Biester, H.; Dittmar, T. *Environ. Sci. Technol.* **2012**, *46*, 4419-4426.
(59) Jiang, J. Y.; Zhang, X. G.; Zhu, X. H.; Li, Y. *Environ. Sci. Technol.* **2017**, *51*, 3435-3444.